



NOVA

University of Newcastle Research Online

nova.newcastle.edu.au

Lee, Soonho; Yu, Jianglong; Mahoney, Merrick; Tremain, Priscilla; Moghtaderi, Behdad; Tahmasebi, Arash; Stanger, Rohan; Wall, Terry; Lucas, John. "Study of chemical structure transition in the plastic layers sampled from a pilot-scale coke oven using a thermogravimetric analyzer coupled with Fourier transform infrared spectrometer". Published in Fuel Vol. 242, Issue 15 April 2019, p. 277-286 (2019)

Available from: <http://dx.doi.org/10.1016/j.fuel.2019.01.024>

© 2019. This manuscript version is made available under the CC-BY-NC-ND 4.0 license
<http://creativecommons.org/licenses/by-nc-nd/4.0/>

Accessed from: <http://hdl.handle.net/1959.13/1401553>

1 Study of chemical structure transition in the plastic layers sampled from a
2 pilot-scale coke oven using a thermogravimetric analyzer coupled with
3 Fourier transform infrared spectrometer

4 Soonho Lee¹, Jianglong Yu^{1,2,*}, Merrick Mahoney¹, Priscilla Tremain¹, Behdad Moghtaderi¹, Arash
5 Tahmasebi^{1,2}, Rohan Stanger¹, Terry Wall¹, John Lucas¹

6 ¹Chemical Engineering, University of Newcastle, Callaghan, NSW 2308, Australia

7 ²Key Laboratory of Advanced Coal and Coking Technology of Liaoning Province, School of
8 Chemical Engineering, University of Science and Technology Liaoning, Anshan 114051, China

9 **Abstract**

10 The aim of this study was to characterize the pyrolysis behavior of the plastic layer formed during the
11 coking process in a 4kg laboratory-scale facility. The 4 kg coke oven was used to produce semi-coked
12 coal samples including the plastic region. The semi-coked samples were scanned by Synchrotron
13 micro-CT to characterize the physical structure changes and identify the sampling locations. Samples
14 corresponding to notional points of softening, maximum fluidity, and resolidification of the plastic
15 layer were obtained for five coking coals of varying thermoplastic properties. Pyrolysis behavior and
16 structural changes of the plastic layer samples were analyzed by a thermogravimetric analyzer coupled
17 with a Fourier transform infrared spectroscopy (TG-FTIR) and an attenuated total reflection Fourier
18 transform infrared spectroscopy (ATR-FTIR). The TG-FTIR analysis allowed the characterization of
19 the changing nature of volatile matter, in which aliphatic and aromatic C-H bonds were observed to
20 undergo the greatest reduction during the plastic layer formation. This was in a line with the ATR-
21 FTIR results which also showed structural changes across the plastic layer. The results suggest that the

* Corresponding author. Email: jianglong.yu@newcastle.edu.au. Tel: +61 2 40333902

22 aliphatic CH bonds of the five coals underwent the greatest reduction with the progression of the plastic
23 layer in the coal charge. One particular observation of interest was that the decomposition trends of
24 the aliphatic CH across the plastic region varied with the thermoplastic properties of the coal samples,
25 implying that the aliphatic structures may play a significant role in the development of plastic
26 properties during the formation of the plastic layer.

27 **Keywords:** Coking coals; Plastic layer; Pyrolysis; TG-FTIR; Chemical structure change.

28 **1. Introduction**

29 Coking coals undergo chemical and physical structure changes during the pyrolysis process inside
30 the coke oven. Thermoplasticity is known as the chemical and physical changes of coking coals in a
31 temperature range of 350-500 °C. As a result of the thermoplasticity, coking coal charge in undergoes
32 a plastic transformation in the coke oven, leading to the formation of a thin plastic layer [1]. The plastic
33 layer consists of the molten vitrinite, non-softened coal components, and tarry products, which are
34 formed during the decomposition of the coal in the thermoplastic range. A further temperature increase
35 causes the cross-linking reactions and thus recodification of the plastic layer to form semi-coke. Taking
36 the process into account, a change in the temperature gradient contributes to the migration of the plastic
37 layer from the heating wall to the center of the coke oven, leaving behind a solid porous residue, i.e.
38 coke. The plastic stage is critical in the coking process as the porosity and the pore wall structure,
39 which significantly affect the coke formation and quality, are mainly determined during this stage [2-
40 4]. Gas entrapment in the plastic layer leads to the generation of the internal gas pressure (IGP), the
41 transmission of which to the oven walls may result in the generation of oven wall pressure (OWP). It
42 is known that high OWPs may cause operational problems, such as serious oven wall damage, the
43 shortening of the battery life time, and increase in the pushing force during coke discharge [5, 6]. For
44 this reason, the pyrolysis coking coals have been extensively studied to predict the behavior inside
45 coke ovens.

46 Generally, coal structure consists of three-dimensional macromolecular networks composed of
47 aromatic sites with grouped aromatic carbons (2-6 rings of average size) [7]. The aromatic sites are
48 cross-linked by aliphatic bridge bonds and oxygen bridges. In the temperature range of 200-400 °C
49 (pre-plastic stage), hydrogen bonds and carboxylic acid decompose, releasing gaseous species such as
50 CO₂ and H₂O. In the plastic range (350-550 °C), weak bridge bonds consisting of the functional groups
51 (i.e., methylene) are ruptured from the macromolecular structure of coal, accompanied by the
52 dealkylation of side chains. This decomposition contributes to the generation of unstable aromatic
53 fragments. The stabilization of generated radicals by hydrogen transfer reactions lead to the production
54 of plastic mass, which has a moderate molecular weight to avoid vaporization [8, 9]. This process is
55 responsible for the exhibition of the fluid-like property in the plastic layer [10]. Several studies
56 suggested that the diameter of the aromatic clusters decreases and the layer spacing increases in the
57 plastic stage due to the disorientation of the aromatic sheets [11, 12]. Some of the aromatic fragments,
58 which are small enough to vaporize are emitted as tars in the plastic layer. Niksa reported that both the
59 plastic mass and the tar are in the molecular weight range of 100-3000 Da [13]. Two kinds of tars can
60 be seen based on the different pyrolysis temperatures [14]. During low-temperature pyrolysis, aromatic
61 and low molecular weight hydrocarbon compounds are mainly present in coal tars. High-temperature
62 coal tars consist of cyclic aromatic hydrocarbon (single ring benzene and alkyl benzene) and aromatic
63 clusters with 20 or more rings [15]. An earlier study suggested that the generated tars pose an influence
64 on the inter-dissolution between non-softened char and plastic mass at the initial softening stage [5].
65 This leads to an increase in the fluidity of the plastic layer by several orders of magnitude. During the
66 primary pyrolysis, the main gases emitted are CO₂, light aliphatic gases, CH₄, and H₂O [16].

67 As the temperature increases above the thermoplastic range (post-plastic stage), the lack of
68 transferable hydrogen in the sequence of stabilizing the radicals causes the plastic mass to cross-link
69 and form char structures. This process is known as the resolidification of the plastic layer [9].
70 Subsequently, the char structures undergo aromatization and condensation of the aromatic clusters

71 with forming polycyclic compounds. This corresponds to the evolution of CH₄ due to the removal of
72 methyl groups from the periphery of the massive char structures. Lastly, further ring condensation
73 gives rise to the evolution of H₂. This post plastic stage involves the rearrangement to the ordered
74 aromatic structures, which increases the size of the aromatic clusters and decreases the layer spacing
75 [11].

76 The migration of the volatile matter generated in the plastic layer has been investigated extensively.
77 It is known that most of the volatile matter (~ 90 %) generated in the plastic layer, escape from the
78 semi-coke side [17, 18]. Among the volatile matter released, the primary tars traverse the coke to the
79 oven wall via the fissures formed in the coke in a temperature range of 600-700 °C. Once the tars reach
80 the oven wall, they travel upwards to space above the coal charge. In the residence time of 20-40 s in
81 the coke and 5 s in the free space, the tar molecules are cracked into light hydrocarbons, hydrogen, and
82 polycondensed aromatic residues at around 800 °C [5]. The rest of the volatile matter generated from
83 the plastic layer (10 %) is released to the cooler side of the plastic layer, i.e. coal side [17, 18]. As
84 previously reported [5], the primary tars in the volatile matter are mainly composed of constituents
85 with high boiling points. When released to the cooler side of the plastic layer, the tar condenses on the
86 surface of the coal particles. The repetition of this process with the migration of the plastic layer causes
87 the heavier fractions of the tars to move toward the center of the coke oven. This increases the fluidity
88 and gradually reduces the softening temperature of the loose coal region ahead of the plastic layer [5].

89 The drawbacks of previous studies in analyzing the pyrolysis behavior in the thermoplastic range
90 are the experimental conditions (i.e., heating conditions and sample size), which may differ from
91 practical coking conditions. This makes it difficult to gain an understanding of the plastic behavior
92 under practical coking conditions. Additionally, the investigations of the migration of the volatile
93 matter have failed to provide detailed chemical structure changes in the plastic layer as it migrates
94 from the oven wall to the center of the coal charge. In this context, it seems that the structural

95 transformation during the formation of the plastic layer is not yet fundamentally understood and
96 requires further investigation.

97 In this study, TG-FTIR analysis was used to measure the changes in the volatiles release as well
98 as the evolution of the aromatic and aliphatic hydrocarbons in the plastic layer. A 4 kg lab scale double-
99 heated wall coke oven, which simulates the one-directional heating conditions inside industrial coke
100 ovens was used to produce semi-coked samples using five Australian coking coals varying with
101 petrographic and thermoplastic properties. The samples consisted of coke/semi-coke, a plastic layer,
102 and loose coal. The plastic region was scanned by Synchrotron micro-CT to show its physical structure
103 transition. Then, sub-samples were extracted from the various locations of the plastic layer, delineated
104 by the micro CT images. TG-FTIR analysis was used to investigate the changes in the rate of mass
105 loss and evolution of the volatile matter components of aromatic and aliphatic hydrocarbons in the
106 sub-samples. When combined with the ATR-FTIR results and cross section micro-CT images, the
107 information obtained in this study allowed a realistic investigation of the changes taking place during
108 the plastic later formation, and thus providing the very much data needed to understand the transition
109 from coal to semi-coke inside the coke oven. This study also identified the parameters of the five coals
110 affecting the pyrolysis behavior of the coal during the plastic layer formation.

111 2. Experimental

112 2.1 Coal samples preparation and characterization

113 The properties of five Australian coking coals used in this study are shown in Table 1. The mean
114 maximum vitrinite reflectance of the coals was in a narrow range of 1.27-1.32, except for the C1 (1.39).
115 The vitrinite contents were in a wider range between 39.6-71.6 %. The ATR-FTIR was employed to
116 analyze the chemical structures of the coals by using structural parameters such as A_{ar}/A_{al} and CH_2/CH_3
117 by following previous studies [19]. The A_{ar}/A_{al} ratio was obtained by integration of characteristic bands
118 of aliphatic and aromatic CH ($3000-2800\text{ cm}^{-1}$ and $3100-3000\text{ cm}^{-1}$). The aliphatic CH band was de-
119 convoluted to obtain the peak areas of CH_2 and CH_3 bands (2920 cm^{-1} and 2950 cm^{-1}) and to calculate

120 the ratio CH_2/CH_3 . Previous finding has suggested that a correlation exists between the structural
 121 parameters and chemical structure of coal [20-22]. The A_{ar}/A_{al} ratio presents the degree of condensation
 122 of the coal structure, which is referred to as the degree of aromaticity, and the CH_2/CH_3 ratio
 123 corresponds to the length or branching degree of aliphatic chains.

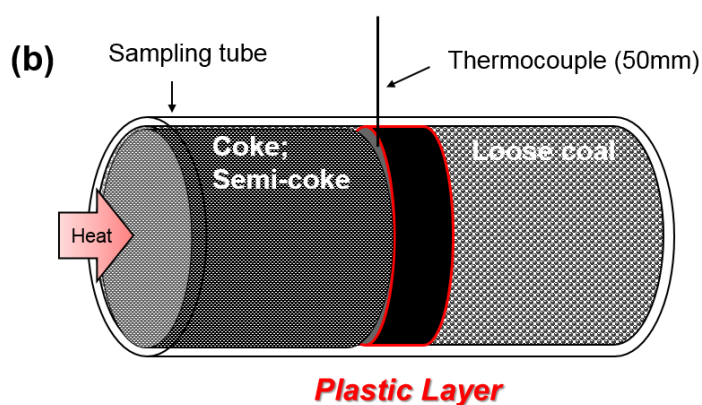
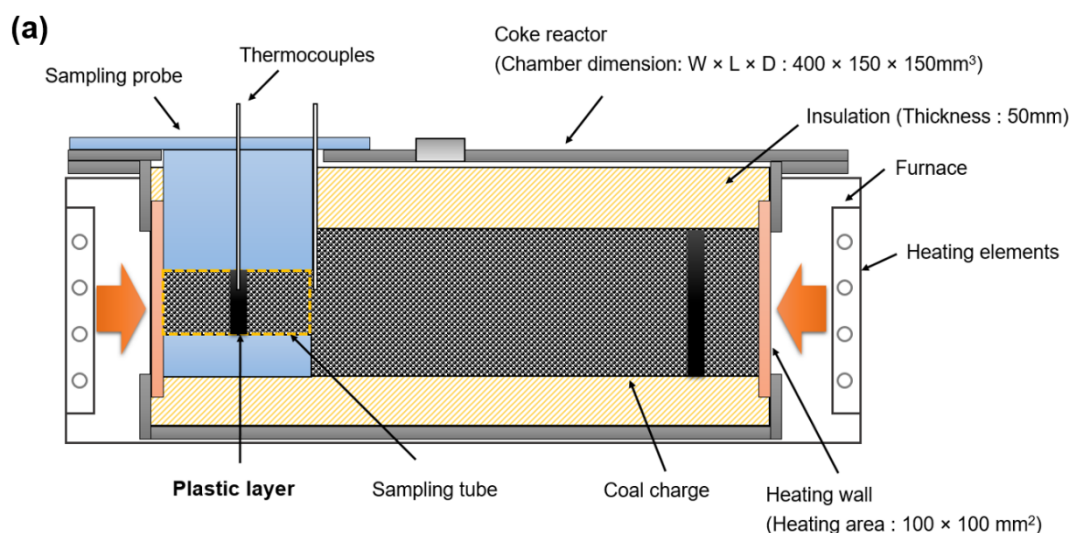
124 **Table 1.** Sample properties and structural parameters (A_{ar}/A_{al} and CH_2/CH_3) of the five Australian
 125 coking coals used to produce the plastic layer samples

Coal samples	C0	C1	C2	C3	C4
Proximate Analysis (ad)					
Inherent Moisture (%)	1.3	1.2	0.9	1.5	2.3
Ash (%)	7.2	8.7	7.8	9.5	7.6
Volatile Matter (%)	22.4	19.5	21.7	22.1	21.2
Fixed Carbon (%)	69.1	70.6	69.6	66.9	68.9
Ultimate Analysis (daf)					
Carbon (%)	88.7	89.9	88.1	88.7	89.2
Hydrogen (%)	5	4.8	5	5	4.8
Nitrogen (%)	2.1	1.7	2.1	2	1.9
Total Sulphur (%)	0.4	0.4	0.6	0.55	0.39
Oxygen (%)	3.8	3.2	4.2	3.8	3.7
Gieseler Fluidity					
Initial Softening Temperature (ST) (°C)	430	435	415	417	428
Max Fluidity Temperature (MFT) (°C)	455	465	460	461	461
Solidification Temperature (RT) (°C)	480	490	495	495	494
Plastic Range (°C)	50	55	80	78	66
Max Fluidity (dd/min)	5	13	189	345	46
Max Fluidity (Log 10)	0.7	1.11	2.28	2.54	1.66
Petrographic analysis					
Mean Maximum Reflectance (%)	1.29	1.39	1.32	1.27	1.31
Vitrinite %	58.9	39.6	61.7	71.6	66
Liptinite %	0.8	\	0.4	0.2	\
Inertinite %	40.3	60.4	37.9	28.2	34
Structural parameters (ATR-FTIR)					
A_{ar}/A_{al}	0.15	0.17	0.13	0.11	0.14
CH_2/CH_3	3.72	3.87	3.19	3.24	3.73

126

127 *2.2 Sampling of plastic layer samples during coking*

128 A 4kg lab-scale coke oven was used to acquire semi-coked coal samples containing the plastic
129 layers under practical heating conditions. As previously reported [19], the key feature of this apparatus
130 was the length of 4 kg coke oven (400 mm) which was similar to that of practical coke ovens.
131 Additionally, insulation enveloped the surface of the coal charge except for the heating wall sides to
132 simulate the one-directional heat transfer from the heating walls (Fig 1(a)). The sampling probe (left
133 side of Fig. 1 (a)) enabled the acquisition of plastic layer samples formed in the practical conditions
134 with the in-situ measurement of temperature profiles at 50 and 100 mm from the heating wall. For
135 sampling plastic layer samples, the received coals were crushed to top 3 mm. Then, the coals were
136 carefully packed in a quartz tube (L: 100 mm, ID: 40 mm) with a controlled charging density of 825
137 kg/m³ as illustrated in Fig. 1 (b). During the packing, a thermocouple was embedded into the coal bed,
138 placed at 50 mm of the quartz tube. The prepared quartz tube is placed into the sampling probe, then
139 inserted into the coke reactor as shown in Fig. 1 (a). The remaining space in the coke reactor was then
140 charged with the same packing density of 825 kg/m³. The heating walls were heated from ambient
141 temperature to 1000 °C at a rate of 10 °C/min. When the temperature at 50 mm reached 500 °C, the
142 sampling probe was removed from the reactor and placed into a cooling chamber purged with nitrogen.
143 The temperature at 50 mm had increased from ambient temperature to 500 °C at a rate of 8 °C/min
144 while the temperature at 100 mm had increased from ambient temperature to 100 °C and dwelled. The
145 semi-coked samples were scanned by Synchrotron micro-CT imaging in a non-destructive way. Then,
146 the incremental extraction as a function of distance from the heating wall was carried out to obtain
147 sub-samples by the method as previously reported [19]. The sub-samples extracted were ground to
148 <62 μm size for the TG-FTIR and ATR-FTIR analyses.



149

150

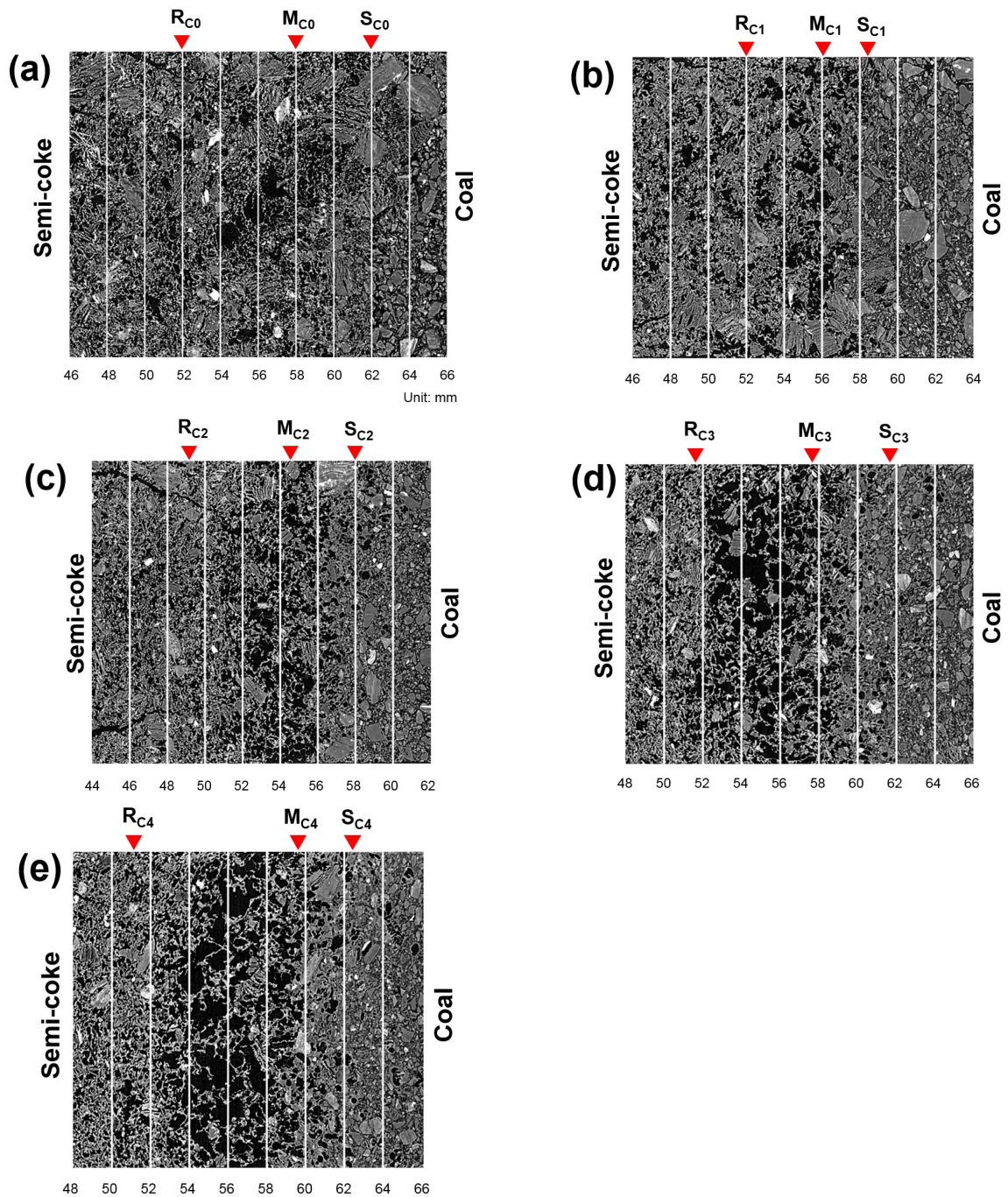
151 **Fig. 1.** The schematic diagram of the 4kg lab-scale coke oven (a) and the sampling tube containing
 152 the plastic layer (b) [19].

153 *2.3 Synchrotron Micro-CT analysis*

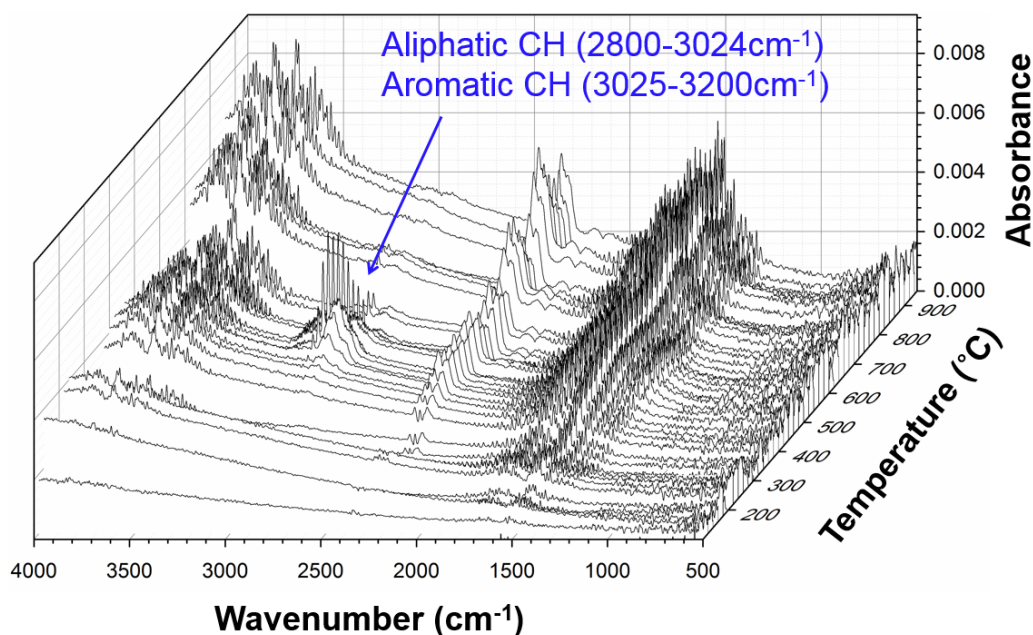
154 The plastic regions in the semi-coked samples were scanned by micro-CT imaging at the Imaging
 155 and Medical Beamline at the Australian Synchrotron, following the previous method [19]. A Ruby
 156 Detector was used, configuring the resolution of each image as 9.81 μm per pixel. The data collection
 157 was performed at an X-ray energy of approximately 30 keV, while the quartz tube containing the
 158 plastic region was rotated over 180 degrees. 6300 vertically stacked slices were acquired to retrieve
 159 the 60 mm height of each plastic region. The retrieval of cross-section images was carried out by
 160 stitching the slices together, using CSIRO's X-TRACT software from the MASSIVE cluster.

161 2.4 TG-FTIR analysis of plastic layer samples

162 **Fig. 2** in the supplementary materials shows that the cross-section images of the semi-coked samples
163 were gridded at 2 mm intervals based on the accurate measurements using Image J software [23]. The
164 red marks (S_{Cn} , M_{Cn} and R_{Cn}) pointed out the approximate locations at which plastic layer samples
165 were extracted, corresponding to notional positions of softening, maximum fluidity and
166 resolidification identified by changes in porosity. The regions right adjacent to S_{Cn} with presenting
167 pore nucleation in the coarse particles were referred to as initial softening layers. The regions between
168 S_{Cn} and M_{Cn} with displaying the initiation of bubble growth were the beginning of intermediate plastic
169 layers. There was dramatic bubble growth between M_{Cn} and R_{Cn} with presenting highest porosity,
170 referred to as intermediate plastic regions. The TG-FTIR was employed to analyze the pyrolysis
171 behavior of the plastic layer samples extracted from S_{Cn} , M_{Cn} and R_{Cn} . The results enabled the
172 investigation of the progressive pyrolysis characteristics inside the plastic layers. About 5 mg of the
173 plastic layer sample was placed in a crucible, then heated to 950 °C at a heating rate of 10 °C/min in a
174 nitrogen atmosphere. FT-IR spectra were recorded by the accumulation of 32 scans with a spectral
175 resolution 4 cm^{-1} for a scan range of 500–4000 cm^{-1} as presented in **Fig. 3**. Online mass loss was
176 measured by the TGA. The evolution of gaseous products, such as aliphatic and aromatic hydrocarbons
177 were monitored by FTIR. The spectral analysis was done by integrating areas under spectral curves of
178 the gaseous products based on the wavenumber assignments (aromatic hydrocarbons: 3025 – 3200 cm^{-1}
179 1 , and aliphatic hydrocarbons: 2800 – 3024 cm^{-1}) [22].



180 **Fig. 2.** Cross section images of the plastic regions with delineating locations of sampling the plastic
 181 layer samples for TG-FTIR analysis ((a): C0, (b): C1, (c): C2, (d) C3 and (e): C4). The red marks
 182 (S_{Cn} , M_{Cn} and R_{Cn}) point to the approximate locations at which plastic layer samples were extracted
 183 and correspond to notional positions of softening, maximum fluidity and resolidification identified
 184 by changes in porosity.



185

186

Fig. 3. FTIR spectra of the volatile matter for the parent coal of C0 during TGA heating.

187

3. Results and discussion

188

3.1 Thermogravimetric analysis of plastic layer

189

190

191

192

193

194

195

196

197

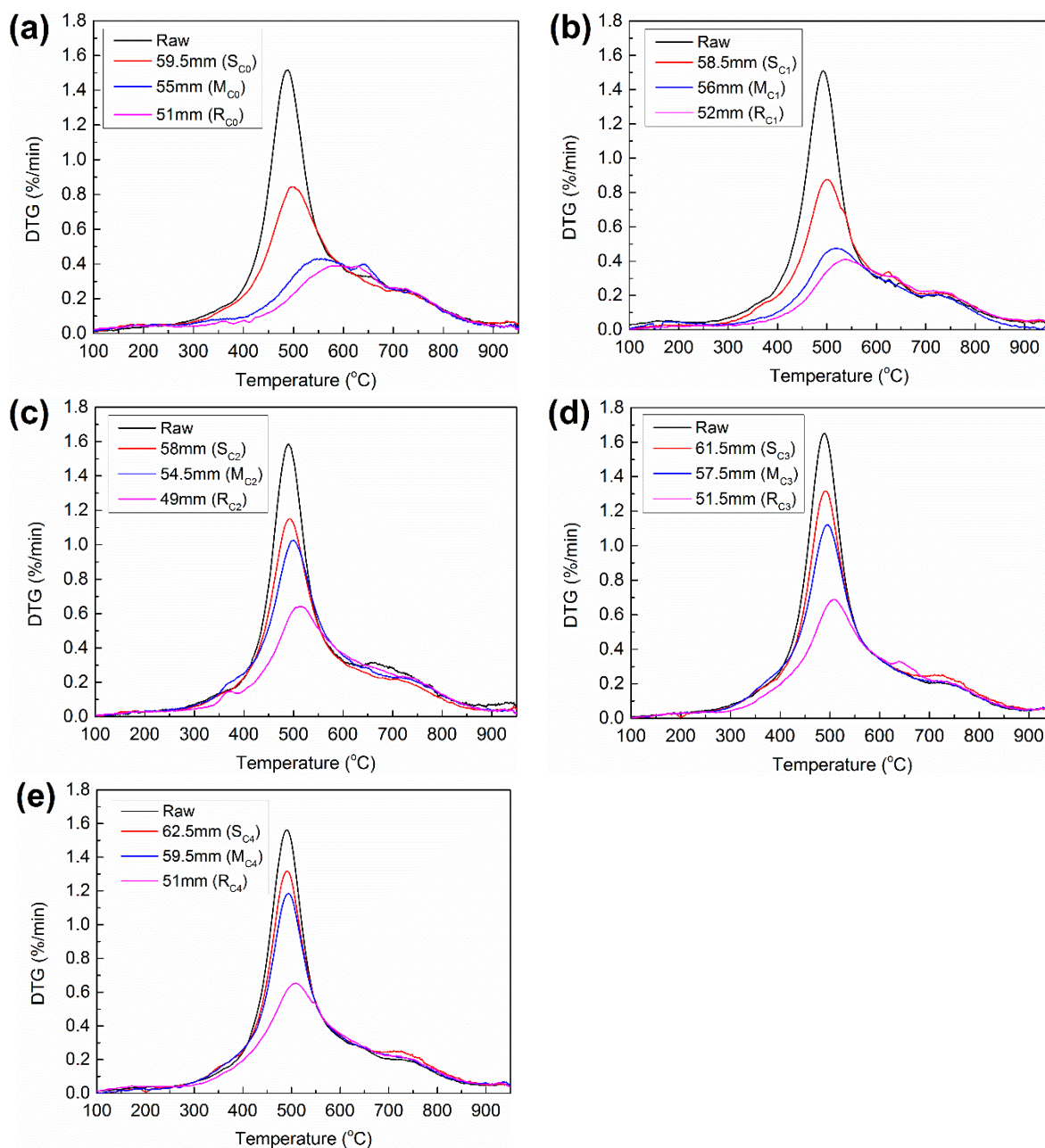
198

199

200

The differential thermogravimetric (DTG) curves of the raw coals and the plastic layer samples are illustrated in [Fig. 4](#). The DTG curves of the raw coals showed that the degree of weight loss varied with temperature, showing a single major peak at about 500 °C. Based on the DTG curves, the pyrolysis process of the raw coals can be divided into several stages. The slight mass loss at temperatures below 200 °C, was attributed to the evolution of adsorbed moisture. With a further temperature increase from 200 °C to 400 °C, a gradual increase in the weight loss rate was evident. As reported earlier [24, 25], this can be attributed to the release of CH₄ and CO₂ due to the rupture of the weaker bonded aliphatic bridges, as well as thermal decomposition of carboxyl groups. The major DTG curve was observed in a temperature range of 400-600 °C. The sharp DTG peaks, which were referred to as the maximum rates of the weight loss (R_{max}), were observed in the temperature range between the maximum fluidity temperatures (MFT) and the resolidification temperatures (ST) (Table 1). These results were consistent with previous findings [26]. The primary devolatilization in this

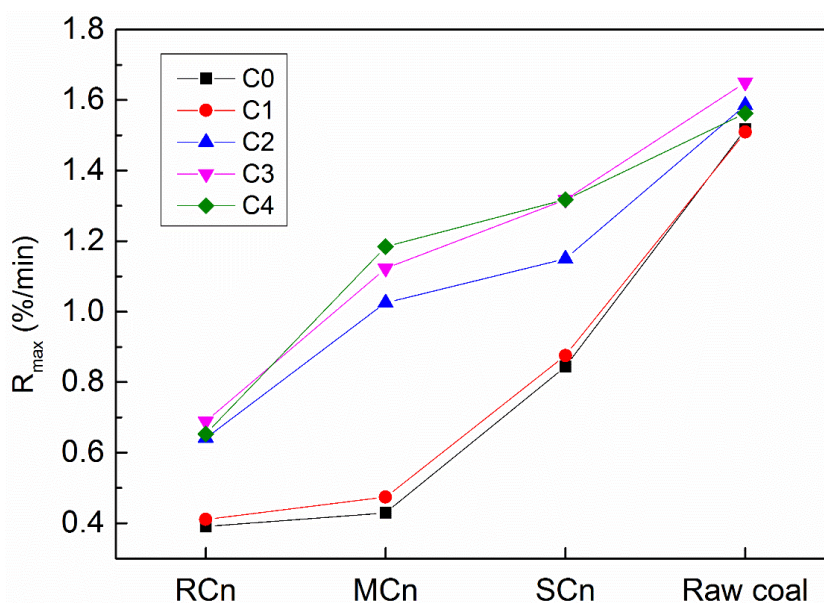
201 temperature range involved the evolution of volatile tar, CH₄, and other light hydrocarbons [27-29].
202 This pyrolysis process involving the devolatilization was consistent with the evolution of aliphatic and
203 aromatic hydrocarbons in the temperate range of 400-700 °C, as detected by the FTIR.



204 **Fig. 4.** Changes in the DTG curves of the raw coals and the sub-samples: (a): C0; (b): C1; (c): C2;
205 (d) C3; and (e): C4.

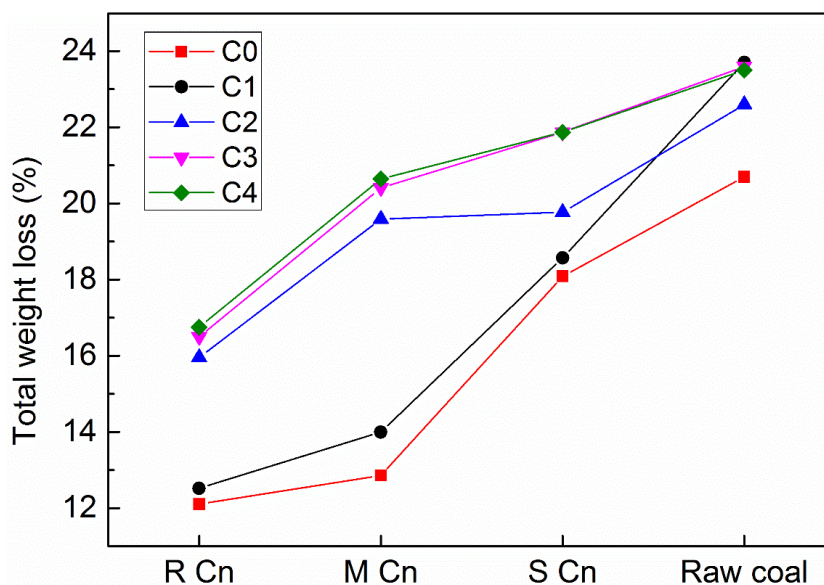
206

207 It is interesting to note that the changes in the intensity of the DTG curves of parent coals and the
 208 corresponding plastic layer samples depended strongly on the fluidity of the coals, as shown in Fig. 4.
 209 Fig. 4 (a) and (b) show that for C0 and C1 coal with lower Gieseler fluidities (Table 1), a more dramatic
 210 decrease in the peak intensities was observed from the initial softening layers ($\sim S_{C0}$ and $\sim S_{C1}$) to the
 211 beginning of the intermediate plastic regions (M_{C0} and M_{C1}). In contrast, for the C2, C3, and C4 coals
 212 with a relatively higher Gieseler fluidity (Table 1), the major changes in the peak intensities were
 213 generally detected in the intermediate plastic regions (i.e. M_{C2} - R_{C2} , M_{C3} - R_{C3} , and M_{C4} - R_{C4}). These
 214 changes in the intensity of peaks are shown as the changes in the R_{max} s and the total weight losses in
 215 Figs. 5 and 6.



216

217 **Fig. 5.** Changes in the maximum rates of the weight losses of the raw coals and the sub-samples
 218 extracted at the boundaries of the characteristic regions (R_{Cn} , M_{Cn} and S_{Cn} were indicated as red in
 219 Fig. 2).



220

221 **Fig. 6.** The total weight losses of the raw coals and the sub-samples extracted from the borders of the
 222 characteristic regions (R_{Cn}, M_{Cn}, and S_{Cn} were indicated as red in Fig. 2).

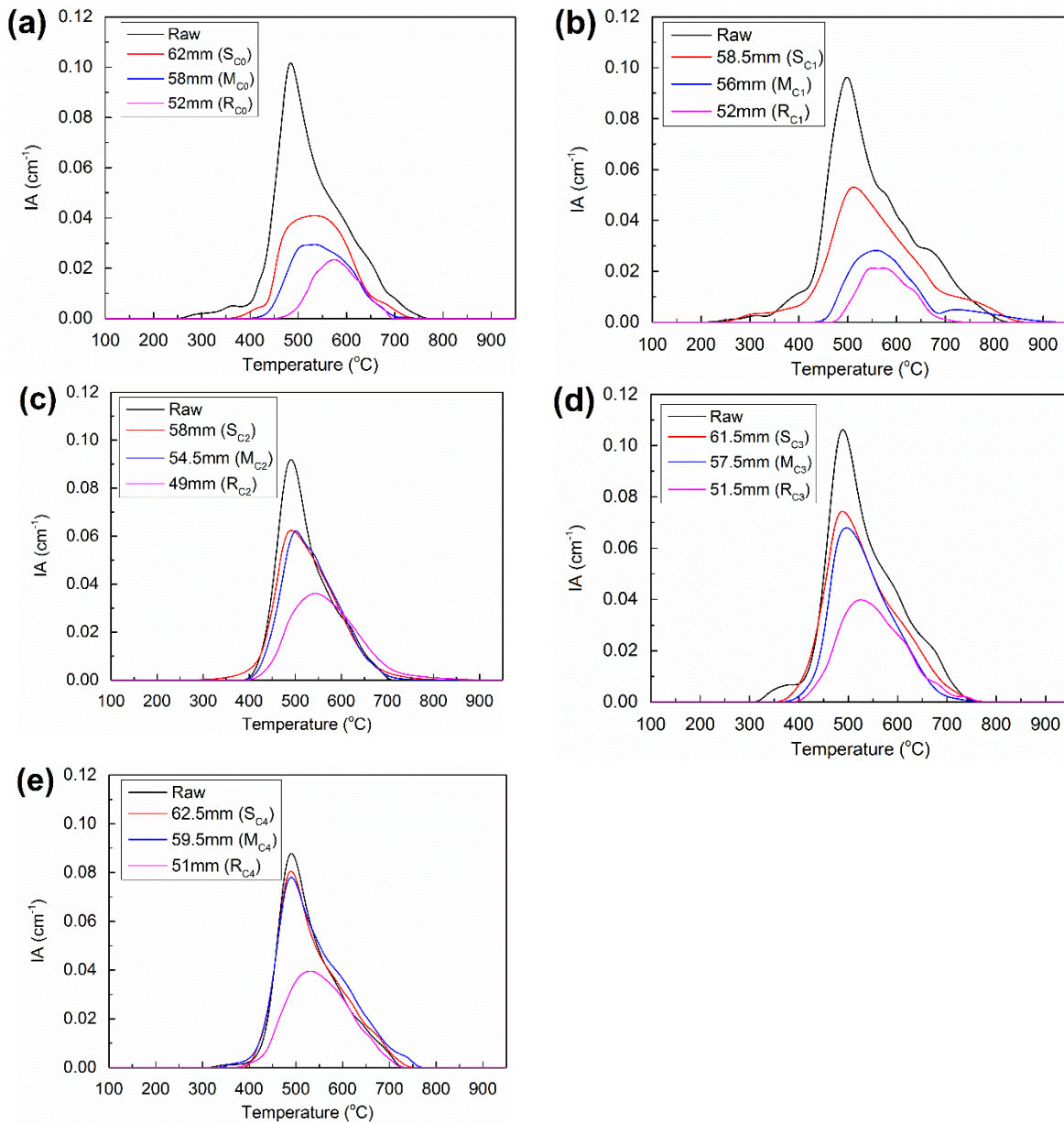
223

224 3.2 FTIR results of the volatile matter from the pyrolysis of the plastic layer samples

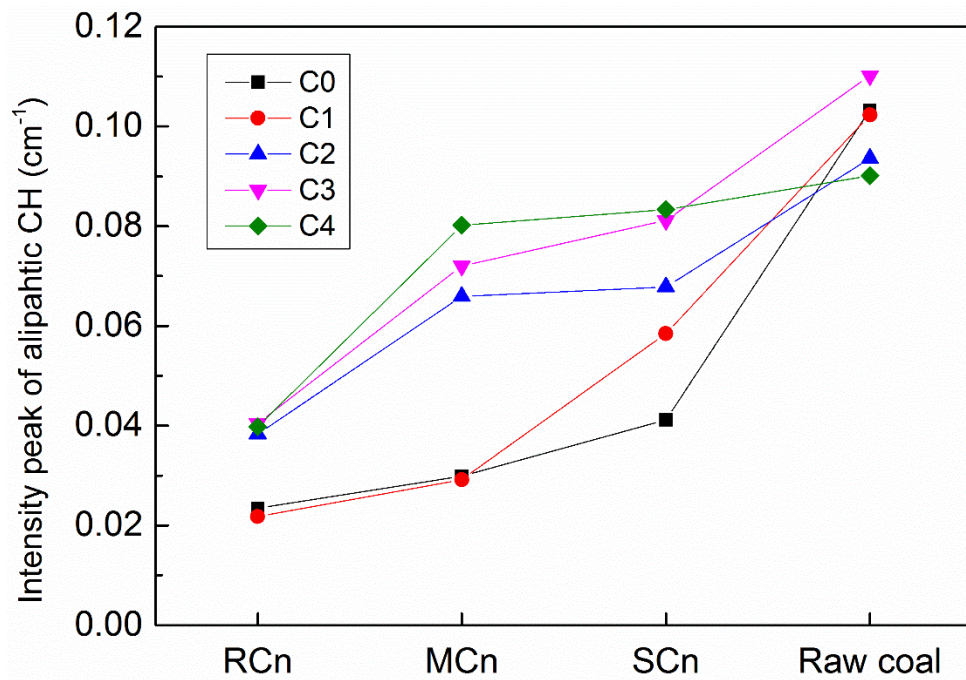
225 **Figs. 7 and 9** present the evolution curves of aromatic and aliphatic hydrocarbons in the parent coals
 226 as well as the corresponding plastic layer samples. Table. 1 shows that the changes in the chemical
 227 structure of the plastic layer estimated by the structural parameters of A_{ar}/A_{al} and CH_2/CH_3 correlated
 228 well with the fluidity properties of parent coals. As shown in Table 1, the C0 and C1 coals (with low
 229 fluidities) contain lower vitrinite contents and the higher rank only for C1. These coals had a higher
 230 A_{ar}/A_{al} and CH_2/CH_3 ratios (Table 1), suggesting the presence of highly condensed aromatic structures
 231 with longer aliphatic chains or lower branching degree of the aliphatic structures [20-22]. The C2 and
 232 C3 coals (with higher fluidities) were of similar rank with higher vitrinite contents, leading to a lower
 233 A_{ar}/A_{al} and CH_2/CH_3 ratios. This implies that the macromolecular structures of C2 and C3 were
 234 composed of less condensed aromatic clusters with shorter aliphatic chains or high branching degree
 235 of aliphatic structures.

236 Fig. 7 shows the evolution of aliphatic hydrocarbons during the TG-FTIR heating of parent coals
237 as well as the sub-samples. The changes in the peak intensity of the evolution curves provide valuable
238 information on the amount of aliphatic hydrocarbon that was released from different characteristic
239 regions such as the initial softening layers and intermediate plastic regions. Figs. 5, 6 and 8 show that
240 the decreasing trends of the peak intensities of the aliphatic hydrocarbons with the progression of the
241 plastic layer were consistent with the decreases in R_{maxS} and the total weight loss, implying that the
242 mass loss of the coal and plastic layer samples were predominantly due to the release of the aliphatic
243 hydrocarbons during the coking process.

244 Fig. 9 shows that the decreasing trends of the peak values of aliphatic hydrocarbons and the DTG
245 curves in the plastic regions varied with the Gieseler maximum fluidity of the parent coals. In case of
246 C0 and C1 coals with the lower Gieseler maximum fluidities, a large decrease in the peak values of
247 the aliphatic hydrocarbons to M_{C0} and M_{C1} were observed, showing a different trend with the higher
248 fluidity coals. These results implied that larger amounts of the aliphatic hydrocarbons were evolved
249 prior to the intermediate plastic layers of the lower fluidity coals. Xiang et al. [20] suggested that coals
250 with higher A_{ar}/A_{al} and CH_2/CH_3 release a larger volume of volatile matters with less amounts of plastic
251 mass produced during the overall pyrolysis process. In this regard, the relatively higher A_{ar}/A_{al} and
252 CH_2/CH_3 of C0 and C1 coals (Table 1) may explain the larger evolution of the aliphatic hydrocarbons
253 at the earlier stages of plastic layer formation. It has been reported that aliphatic components within
254 the coal macromolecule play an important role in stabilizing the radicals generated during the thermal
255 decomposition of coal in a thermoplastic range producing moderate molecular weights, referred to as
256 plastic mass [30, 31]. In this context, it is possible that the earlier removal of the aliphatic components
257 ahead of the intermediate plastic layer formation led to the lack of donable hydrogen in the intermediate
258 plastic regions, thus generating less amount of the plastic mass. Such lower fluid-like properties lead
259 to less entrapment of gases in the plastic region, resulting in lower porosities as reported in the previous
260 study by the authors on the image analysis of the micro-CT images (Fig. 2) [19].



261 **Fig. 7.** Changes in the evolution of the aliphatic hydrocarbons for the raw coals and the sub-samples,
 262 monitored by the FTIR ((a): C0, (b): C1, (c): C2, (d) C3 and (e): C4).

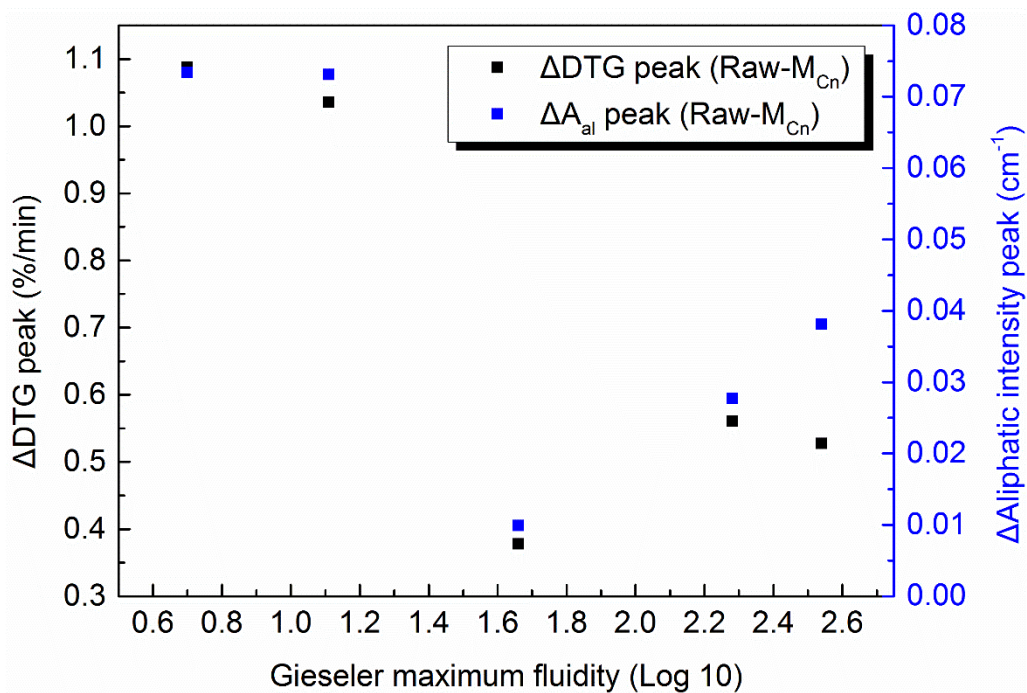


263

264 **Fig. 8.** Changes in the intensity peaks of the aliphatic hydrocarbons for the raw coals and the sub-

265

samples.



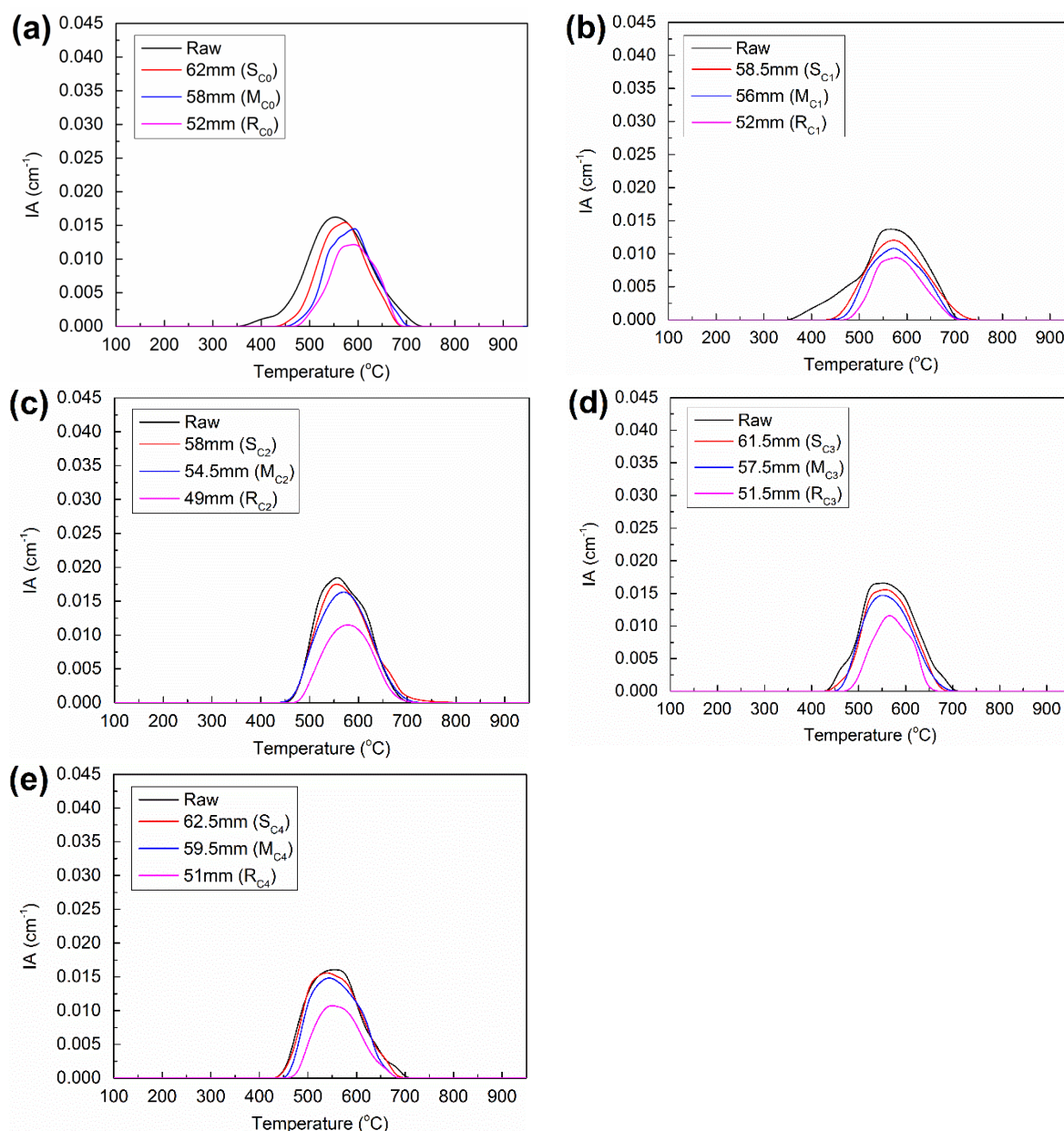
266

267 **Fig. 9.** Correlation between the Gieseler maximum fluidities and changes in the DTG peaks and the

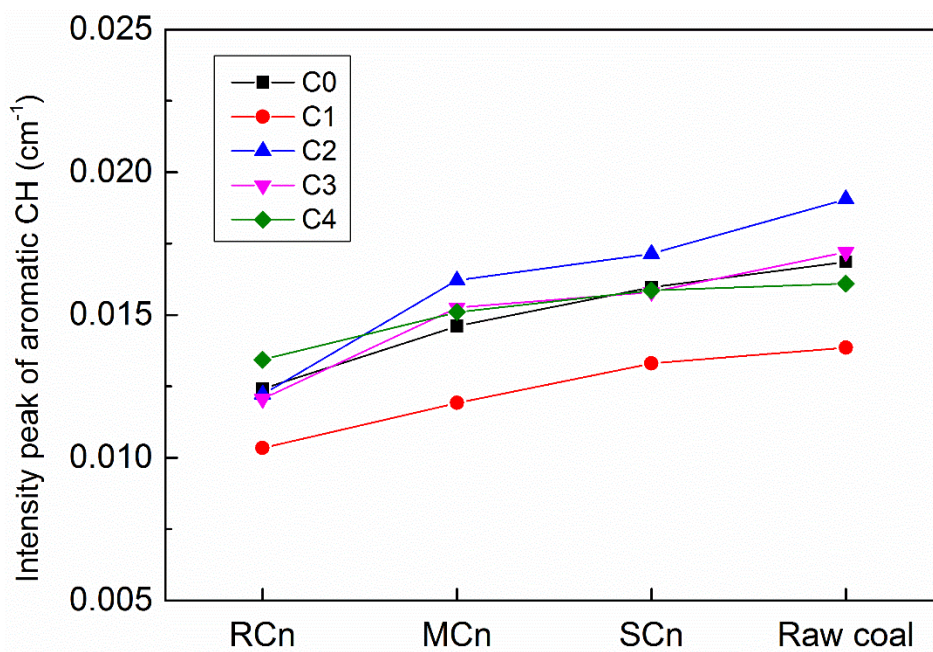
268

aliphatic intensity peaks between the parent coals and the sub-samples at M_{Cn}.

269 **Fig. 10** presents the changes in the evolution of aromatic hydrocarbons from the raw coals and the
 270 plastic layer samples. The evolved aromatic hydrocarbons are considered as major tar components. As
 271 previously suggested, tars consist of aromatic hydrocarbons with alkyl-substituents [32]. **Fig. 11** shows
 272 that the intensities of the aromatic CH peak gradually decreased across the plastic layer, but show little
 273 variations between different coals (except C1 which appeared lower for all samples).



274 **Fig. 10.** Changes in the evolution of the aromatic hydrocarbons for the raw coals and plastic layer
 275 samples as measured by the FTIR: (a): C0; (b): C1; (c): C2; (d) C3; and (e): C4.



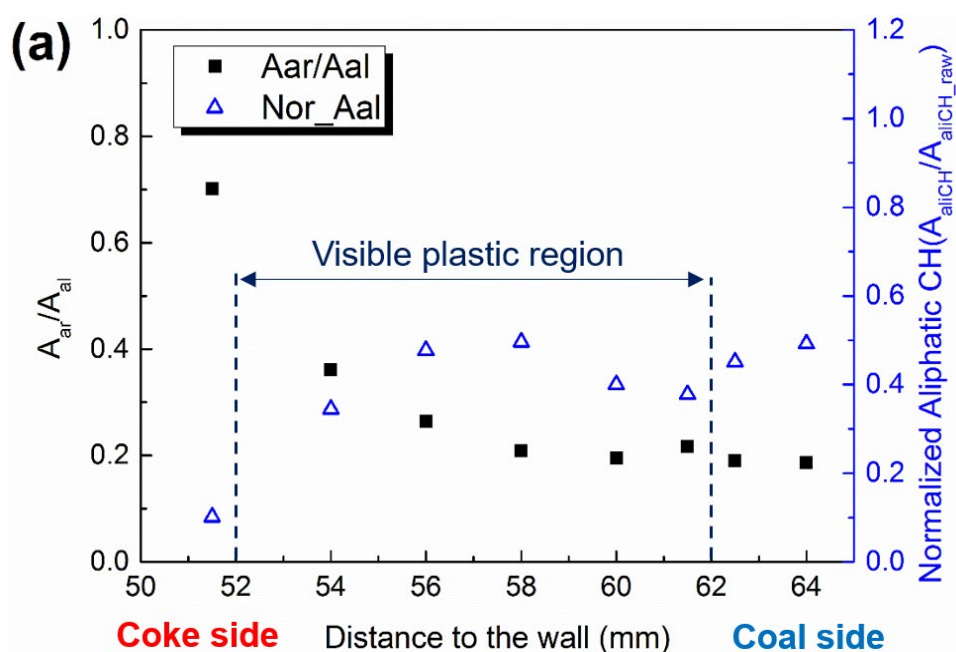
276

277 **Fig. 11.** Changes in the intensity peaks of the aromatic hydrocarbons for the raw coals and the sub-
 278 samples.

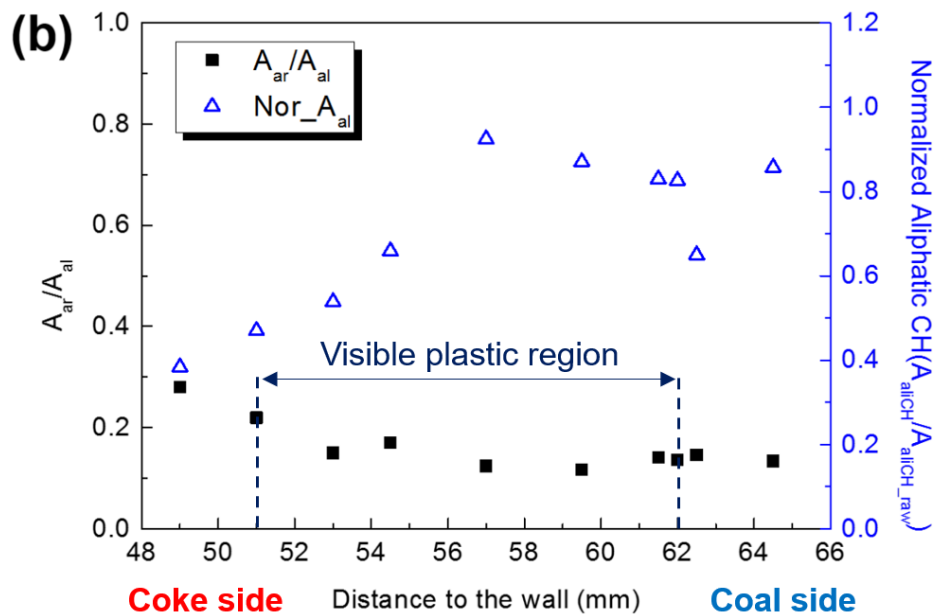
279 *3.3 ATR-FTIR analysis of the chemical structure changes across the plastic layer*

280 The ATR-FTIR analysis results showed that in C0 and C4 coals the pyrolysis behavior in the initial
 281 softening layers was in a good agreement with the structural transformation inside the plastic layers
 282 (Fig. 12). The ATR-FTIR results for samples C1, C2, and C3 were presented in our previous study
 283 [19]. The ATR-FTIR results for the C0 and C4 coals in Fig. 12 are calculated based on the ratio of
 284 aromatic CH to aliphatic CH signal intensities in plastic layer samples (A_{ar}/A_{al}) as well as the ratio of
 285 the aliphatic CH in the plastic layer samples to the aliphatic CH in the raw coal ($N_{or} A_{al}$). As seen in
 286 Fig. 12, the A_{ar}/A_{al} ratio showed an overall increasing trend across the visible plastic layer from the
 287 coal side to the coke side for both C0 and C4 coals. The normalized aliphatic CH was decreased at the
 288 coal sides of the visible plastic regions. This was followed by a relatively constant stage and finally a
 289 drastic decrease on the coke side of the plastic layer. These changes were consistent with a loss of
 290 bonds throughout the devolatilization process and increasing aromatization of the semi-coke structure.
 291 However, the level of response appears to vary with fluidity level of the parent coal. Fig. 12 shows
 292 that the lowest fluidity C0 coal underwent a larger change in the concentration of aliphatic CH groups

293 on the coal side of the plastic region during the devolatilization (see Fig. 7 (a)), compared to the higher
 294 fluidity C4 coal (see Fig. 7 (e)). The A_{ar}/A_{al} value the lowest fluidity C0 coal increased drastically from
 295 0.2 to 0.7 across the plastic layer, while in case of the higher fluidity C4 coal only a slight change from
 296 0.15 to 0.3 was observed. The ATR-FITR analysis results for the C1 (low fluidity), C2, and C3 (higher
 297 fluidity) coals in our previous study [19] showed that the changes in the A_{ar}/A_{al} ratio and the aliphatic
 298 CH were also dependent on the fluidity of the parent coal. These results suggested that the higher
 299 fluidity coals (C2, C3, and C4) contain higher levels of aliphatic CH structures, which may in turn
 300 potentially cause further depolymerization in the plastic regions.



301



302

303 **Fig. 12.** ATR-FTIR analysis of the changes in the structural parameters (A_{ar}/A_{al} and normalized
 304 aliphatic CH) across the plastic layers: (a): C0; and (b): C4. Visible plastic region refers to higher
 305 porosity region identified by Synchrotron micro-CT scans, noting that the hot side of the coke oven
 306 is closest to the wall and that lower temperatures are encountered with increasing distance from the
 307 wall.

308 3.4 Discussion on behavior across the plastic layer and coal properties

309 This work has detailed a novel methodology to obtain the representative plastic layer samples
 310 formed under the practical heating conditions in the 4kg laboratory scale system. The plastic layer
 311 samples were analyzed by the combination of analytical techniques such as TG-FTIR, ATR-FTIR and
 312 micro-CT scanning. This provides the opportunity to characterize pyrolysis behavior of coking coals,
 313 in particular the chemical structure changes across the plastic layer formed during the coking process.
 314 It was shown that the level of volatile matter was reduced in the plastic layer samples corresponding
 315 to the notional points of softening, maximum fluidity, and resolidification which took place during the
 316 coking of five coking coals of varying thermoplastic properties.

317 Of particular interest was the changing of the nature of volatile matter as characterized by FTIR,
318 which showed that the aliphatic C-H structures were underwent the greatest reduction across the plastic
319 layer. The aromatic C-H structures appeared to be relatively unchanged with only minor reduction
320 across the plastic layer. These results suggested that the aliphatic functionalities in coal may play a
321 significant role in the development of plastic properties and subsequent semi-coke formation inside
322 the coke oven. It is not yet clear whether this observed change in aliphatic bonding is caused by the
323 aliphatic species or tar species with aliphatic side chains. However, the structural changes observed in
324 the solid samples in the lead up to the resolidification appeared to support the notion of increasing
325 aromatisation at the expense of aliphatic content (reporting to the volatiles).

326 The pyrolysis concepts governing this process are well known, but difficult to translate to the
327 performance of individual coals undergoing one-dimensional heat transfer in a coke oven. This work
328 has attempted to link the changes in the bulk thermoplastic properties to the chemical structure in both
329 solid and volatile phases. There is a consensus that the physical structure of the coke is determined to
330 a large extent during the plastic layer formation and migration to the centre of the coal charge. This
331 has direct implications on the quality of the resultant coke in terms of reactivity and strength. Despite
332 the critical role of plastic layer in shaping the final quality of the coke, the exact mechanism of the
333 changes in the chemical structure of coal as it transitions from coal to semi-coke during the plastic
334 later formation is not well understood and therefore was the major subject of this study. The findings
335 of this study sheds light on the chemical structure transition inside the plastic layer from that of coal
336 to semi-coke. The major finding was that the formation of the plastic layer is closely associated with
337 the removal of aliphatic CH from coal structure. Further research is required for linking such chemical
338 change to the finer features of coke structure to better understand the impact of chemical structure
339 changes during the plastic layer formation to the strength and reactivity of the final coke product.

340 **4. Conclusions**

- 341 • This study has characterized the pyrolysis behavior of the plastic layer formed in a 4kg coke
342 oven which simulated practical heating conditions. The TG-FTIR and ATR-FTIR were used to
343 analyze the plastic layer samples of five coking coals of varying thermoplastic properties.
- 344 • The TG-FTIR results implied that the level of aliphatic hydrocarbons in the volatile phase was
345 generally reduced in the plastic layer samples corresponding to the notional points of softening,
346 maximum fluidity and resolidification. Meanwhile, Aromatic C-H structures appeared to
347 remain relatively unchanged across the plastic layer. This was in a good agreement with the
348 structural changes of the solid samples, as analyzed by ATR-FTIR.
- 349 • Comparing the decomposition trends of the aliphatic structures in the five coals tested, it was
350 observed that the higher fluidity coals showed a smaller reduction in the aliphatic CH structures
351 at the beginning of the plastic regions via the evolution of aliphatic hydrocarbons. Subsequently,
352 the aliphatic CH bonds were largely decreased in the intermediate plastic region. In contrast,
353 the low fluidity coals presented the larger decreases in aliphatic CH bonds to the beginning of
354 the plastic regions via the release of aliphatic hydrocarbons. This suggests that the different
355 decomposition trends of the aliphatic structures may pose a strong impact on the development
356 of plastic properties during the formation of the plastic layers.

357 **Acknowledgments**

358 This research was financially supported by the ACARP (Australian coal industry's Research
359 Program). We also wish to acknowledge the tremendous technical supports from industrial mentors,
360 Mr. Kim Hockings at BHP, Mr. Chris Stanford formerly at Peabody Energy, and Mr. Sean Flanagan
361 of Wesfarmers Curragh. The Micro-CT imaging analysis was undertaken on the Imaging and Medical
362 Beamline (IMBL) at the Australian Synchrotron, part of ANSTO. We thank Dr Anton Maksimenko,
363 IMBL, Australian Synchrotron for his assistance and support in recording micro-CT images.

364 **References**

- 365 [1] Alvarez R, Díaz-Estébonez M. Chemistry of production of metallurgical coke. Sciences of Carbon
366 Materials (Marsh, H, Rodríguez-Reinoso, F, eds) Universidad de Alicante, Alicante, Spain 2000.
- 367 [2] Fuller Jr E. Coal and coal products: analytical characterization techniques. ACS Symposium
368 Series 205. 1982.
- 369 [3] Hays D, Patrick JW, Walker A. Pore structure development during coal carbonization. 1.
370 Behaviour of single coals. Fuel 1976;55(4):297-302.
- 371 [4] Marsh H, Clarke D. Mechanism of formation of structure within metallurgical coke and its effect
372 on coke properties. Erdol und Kohle 1986;39(s 113).
- 373 [5] Loison R, Foch P, Boyer A. Coke: quality and production. Elsevier; 2014.
- 374 [6] Guelton N, Rozhkova TV. Prediction of coke oven wall pressure. Fuel 2015;139:692-703.
- 375 [7] Smith KL, Smoot LD, Fletcher TH, Pugmire RJ. The structure and reaction processes of coal.
376 Springer Science & Business Media; 2013.
- 377 [8] Nomura M, Kidena K, Hiro M, Murata S. Mechanistic study on the plastic phenomena of coal.
378 Energy Fuels 2000;14(4):904-9.
- 379 [9] Grint A, Mehani S, Trewhella M, Crook MJ. Role and composition of the mobile phase in coal.
380 Fuel 1985;64(10):1355-61.
- 381 [10] Genetti DB. An advanced model of coal devolatilization based on chemical structure. Brigham
382 Young University. Department of Chemical Engineering; 1999.
- 383 [11] Kidena K, Murata S, Nomura M. Studies on the chemical structural change during carbonization
384 process. Energy Fuels 1996;10(3):672-8.
- 385 [12] Wang S, Chen H, Ma W, Liu P, Yang Z. Structural Transformations of Coal Components upon
386 Heat Treatment and Explanation on Their Abnormal Thermal Behaviors. Energy Fuels
387 2017;31(11):11587-93.

- 388 [13] Niksa S. Rapid coal devolatilization as an equilibrium flash distillation. *AIChE J* 1988;34(5):790-
389 802.
- 390 [14] Elliott MA. Chemistry of coal utilization. Second supplementary volume. 1981:1006-83.
- 391 [15] McNeil D. High-temperature coal tar. Chemistry of coal utilization 2nd suppl vol New York (NY):
392 John Wiley and Sons 1981:1003-83.
- 393 [16] Solomon PR, Hamblen DG, Carangelo R, Serio M, Deshpande G. General model of coal
394 devolatilization. *Energy Fuels* 1988;2(4):405-22.
- 395 [17] Aramaki T, Edakuni T, Sekine H, Komaki I, Kojima T. Study of Gas Flow Pattern in Coke Oven
396 Chamber and Its Effect on Coking Process. *Ironmaking Conference Proceedings*. 50. 1991:147-
397 53.
- 398 [18] Latshaw G, McCollum H, Stanley R. Wall pressure determination by measurement and
399 interpretation of internal gas pressures in a six-meter coke battery. *Ironmaking Proceedings*. 43.
400 1984:373-80.
- 401 [19] Lee S, Yu J, Mahoney M, Tremain P, Moghtaderi B, Tahmasebi A. A study on the structural
402 transition in the plastic layer during coking of Australian coking coals using Synchrotron micro-
403 CT and ATR-FTIR. *Fuel* 2018;233:877-84.
- 404 [20] Xiang L, Qin Z, Bu L, Zhuang Y, Shen C. Structural analysis of functional group and mechanism
405 investigation of caking property of coking coal. *J Fuel Chem Technol* 2016;44(4):385-93.
- 406 [21] Ibarra J, Munoz E, Moliner R. FTIR study of the evolution of coal structure during the
407 coalification process. *Org Geochem* 1996;24(6-7):725-35.
- 408 [22] Orrego J, Cabanzo Hernández R, Mejía-Ospino E. Structural study of colombian coal by fourier
409 transform infrared spectroscopy coupled to attenuated total reflectance (FTIR-ATR). *Revista*
410 *mexicana de física* 2010;56(3):251-4.
- 411 [23] Schneider CA, Rasband WS, Eliceiri KW. NIH Image to ImageJ: 25 years of image analysis. *Nat*
412 *Methods* 2012;9(7):671.

- 413 [24] Arenillas A, Rubiera F, Pis J. Simultaneous thermogravimetric–mass spectrometric study on the
414 pyrolysis behaviour of different rank coals. *J Anal Appl Pyrol* 1999;50(1):31-46.
- 415 [25] Liu J, Jiang X, Shen J, Zhang H. Pyrolysis of superfine pulverized coal. Part 1. Mechanisms of
416 methane formation. *Energy Convers Manage* 2014;87:1027-38.
- 417 [26] Komaki I, Itagaki S, Miura T. Structure and thermoplasticity of coal. Nova Publishers; 2005.
- 418 [27] Shi L, Liu Q, Guo X, Wu W, Liu Z. Pyrolysis behavior and bonding information of coal-a TGA
419 study. *Fuel Process Technol* 2013;108:125-32.
- 420 [28] Solomon P, Serio M, Carangelo R, Bassilakis R, Gravel D, Baillargeon M, et al. Analysis of the
421 Argonne premium coal samples by thermogravimetric Fourier transform infrared spectroscopy.
422 *Energy Fuels* 1990;4(3):319-33.
- 423 [29] Xie W, Wall T, Lucas J, Mahoney M, Stanger R. Chemical Changes of Australian Coking Coals
424 from Different Basins with Various Ranks and Maceral Compositions: Linking to Both Physical
425 and Thermal Changes. *Energy Fuels* 2016;30(12):10136-47.
- 426 [30] He Y, Zhao R, Yan L, Bai Y, Li F. The effect of low molecular weight compounds in coal on the
427 formation of light aromatics during coal pyrolysis. *J Anal Appl Pyrol* 2017;123:49-55.
- 428 [31] Qiu S, Zhang S, Wu Y, Qiu G, Sun C, Zhang Q, et al. Structural transformation of fluid phase
429 extracted from coal matrix during thermoplastic stage of coal pyrolysis. *Fuel* 2018;232:374-83.
- 430 [32] Strezov V, Morrison A, Nelson P. Thermal Study of the Coking Behaviour of Thermoplastic Coals.
431 Macquarie University: Sydney, Australia; 2007.